Phys Chem Minerals (2003) 30: 88–97
DOI 10.1007/s00269-002-0294-y

ORIGINAL PAPER

B. P. Burton · A. Van de Walle

First-principles-based calculations of the $CaCO_3$–$MgCO_3$ and $CdCO_3$–$MgCO_3$ subsolidus phase diagrams

Received: 6 May 2002 / Accepted: 23 October 2002

Abstract Planewave pseudopotential calculations of supercell total energies were used as bases for first-principles calculations of the $CaCO_3$–$MgCO_3$ and $CdCO_3$–$MgCO_3$ phase diagrams. Calculated phase diagrams are in qualitative to semiquantitative agreement with experiment. Two unobserved phases, $Cd_3Mg(CO_3)_4$ and $CdMg_3(CO_3)_4$, are predicted. No new phases are predicted in the $CaCO_3$–$MgCO_3$ system, but a low-lying metastable $Ca_3Mg(CO_3)_4$ state, analogous to the $Cd_3Mg(CO_3)_4$ phase is predicted. All of the predicted lowest-lying metastable states, except for huntite $CaMg_3(CO_3)_4$, have dolomite-related structures, i.e. they are layer structures in which A_mB_n cation layers lie perpendicular to the rhombohedral [111] vector.

Keywords First principles · Phase diagram calculation · Order–disorder · $CaCO_3$–$MgCO_3$ · $CdCO_3$–$MgCO_3$

Introduction

Experiments by Goldsmith and coworkers (Goldsmith and Heard 1961; Goldsmith 1972, 1983) elucidated phase relations in the systems calcite–magnesite, $X \cdot CaCO_3 - (1-X) \cdot MgCO_3$, and otavite–magnesite, $X \cdot CdCO_3 - (1-X) \cdot MgCO_3$ ($X =$ mol fraction $MgCO_3$) and established the characteristic phase diagram topology: a relatively narrow homogeneity range for an ordered dolomite structure phase that transforms by a second-order transition to a disordered calcite structure phase; broad calcite + dolomite two-phase fields flank the dolomite homogeneity range. Previous phase-diagram calculations (Navrotsky and Louks 1977; Burton and Kikuchi 1984; Burton 1987; Burton and Davidson 1988) for these and related systems (e.g. $CaCO_3$–$FeCO_3$, Davidson 1994) were based on empirically derived Hamiltonians (sets of energy parameters) and directed towards: (1) finding a minimal model that qualitatively reproduces phase-diagram topology and (2) fitting experimental phase equilibria and thermochemical data (Navrotsky and Capobianco 1987; Capobianco et al. 1987; Chai et al. 1995). This paper presents first-principles (FP) phase-diagram (FPPD) calculations in which cluster expansion (CE) Hamiltonians (Sanchez et al. 1984; McCormack and Burton 1997) are fit to sets of supercell total energies ($\{E_{Str}\}$, where *Str* indicates the crystal structure) that were calculated with a plane wave pseudopotential code (Kresse and Hafner 1993).

The calcite crystal structure (calcite, otavite, magnesite) can be idealized as interpenetrating face-centered cubic (*fcc*) substructures of cations (Ca^{2+}, Cd^{2+}, Mg^{2+}), and planar CO_3^{2-} anion groups. One $[111]_{fcc}$ vector becomes the rhombohedral three fold axis ($[111] \equiv [111]_{fcc} = [111]_{rhom} = [0001]_{hex}$) because the planes defined by CO_3 groups lie in the perpendicular (111) plane [$(111) \equiv (111)_{fcc} = (111)_{rhom} = (0001)_{hex}$]. In the dolomite structures [$CaMg(CO_3)_2$ and $CdMg(CO_3)_2$], alternating (111) planes are occupied by different cations (e.g. dolomite, Ca–Mg–Ca– etc.), which reduces space-group symmetry from $R\bar{3}c$ in calcite to $R\bar{3}$ in dolomite. In both calcite and dolomite, the CO_3 groups are ordered such that all groups in the same (111) plane have the same orientation, and groups on neighboring (111) planes are oriented in an opposite sense.

In the $CaCO_3$–$MgCO_3$ system, some additional ordered superstructures have been predicted as possible equilibrium phases (Burton 1987), or reported as metastable phases in natural samples of magnesian calcite, calcian dolomite, or ankerite [$Ca(Fe,Ca,Mg)(CO_3)_2$ with dolomite structure; Van Tendeloo et al. 1985; Wenk and Zhang 1985; Meike et al. 1988; Reksten 1990a,b,c)].

B. P. Burton (✉)
Materials Science and Engineering Laboratory,
Ceramics Division National Institute of Standards
and Technology, Gaithersburg, Maryland 20899, USA
e-mail: benjamin.burton@nist.gov

A. Van de Walle
Materials Science and Engineering Department,
Northwestern University 633 Clark Street Evanston,
Illinois 60208, USA
e-mail: avdw@northwestern.edu

Several superstructures can be described in terms of analogous Fcc-based ordered alloy structures (Burton and Davidson 1988; Wenk et al. 1991; Table 1). Huntite [$\mathcal{H}'$, $CaMg_3(CO_3)_4$; Graf and Bradley 1962] occurs in nature, and it exhibits $CuAu_3$-type ordering of both cations (as in μ') and CO_3 anion groups. Unlike calcite, dolomite, or other superstructures considered here, the CO_3 groups in huntite are orientationally ordered both between and within (111) anion layers. There are also dolomite-related layer structures that consist of various sequences of Ca- and Mg-rich layers perpendicular to [111] (Table 2).

Two factors that significantly affect carbonate phase relations are ignored in this study: (1) CO_3 group orientational order disorder; (2) quasiternary cation substitutions. The former is known to occur in $CaCO_3$ (and magnesian calcite), which exhibits a phase transition at ~1260 K (Dove and Powell 1989). Such transitions have not been reported in $CdCO_3$ or $MgCO_3$. Factor (2) above primarily affects the comparison of FPPD calculations for the pure $CaCO_3$–$MgCO_3$ systems with electron microscopy studies of natural samples that contain significant concentrations of transition metals, particularly Fe; e.g. the natural samples described in Wenk et al. (1991) have compositions $Ca_{0.5}Mg_{0.2}Fe_{0.3}CO_3$ and $Ca_{0.95}Mg_{0.05}CO_3$.

The prediction in Burton (1987) was for a possible low-temperature equilibrium $Ca_3Mg(CO_3)_4$ phase with either μ (Cu_3Au) or ζ (Al_3Ti)-related ordering, or a combination of the two (Burton and Davidson 1988). Wenk et al. (1991) report the unequivocal observation of δ in calcian dolomite, and suggest that γ is most probably the source of **c** reflections, which occur halfway between fundamental reflections along a_1 hexagonal (e.g. at $h-\frac{1}{2}hl$, Table 2 in Van Tendaloo et al. 1982) and are associated with intralayer ordering, in magnesian calcite; ν-type ordering is also proposed as a possible cause of **c** reflections. The FP and FPPD results presented below include formation energies for all these structures and, assuming that cation ordering is the only relevant process, (1) predict no stable intermediate phases between calcite and magnesite; (2) confirm that δ is a low-energy candidate for metastable formation from calcian dolomite; (3) appear to rule out γ, μ, ν, and ζ as plausible candidates for metastable formation; (4) Predict that ϵ is the lowest-lying metastable state at $X=\frac{1}{4}$.

Table 1 Fcc-related crystal structures

Name[a]	Symbol[b]	X	Space group[c]	*FCC*-related prototype
α	•	0	$R\bar{3}c$	*fCC* calcite
γ	▽	$\frac{1}{4}$	$P\bar{1}$	Cu_3Pt
ζ	▲	$\frac{1}{4}$	$C2/c$	Al_3Ti
μ	×	$\frac{1}{4}$	$R\bar{3}c$	Cu_3Au
ν	○	$\frac{1}{2}$	$C2/c$	CuAu
β	■	$\frac{1}{2}$	$R\bar{3}$	CuPt dolomite
$\mathcal{H}'$	◁	$\frac{3}{4}$	$R32$	$CuAu_3$ huntite[d]

[a] A complimentary structure in which Ca or Cd is replaced by Mg and vice versa, is distinguished by a primed name; e.g μ is $Ca_3Mg(CO_3)_4$ ($X=\frac{1}{4}$), μ' is $CaMg_3(CO_3)_4$ ($X=\frac{3}{4}$)
[b] Symbols used in Figs. 1 and 2
[c] Space group determinations were performed with the Cerius program
[d] Huntite has $CuAu_3$-type cation order as in μ', but its CO_3 groups are ordered differently from those in calcite, dolomite, or other supercells considered here

Total energy calculations

Total energies, E_{Str}, were calculated for $CaCO_3$, $CdCO_3$, $MgCO_3$, and many $Ca_mMg_n(CO_3)_{(m+n)}$ and $Cd_mMg_n(CO_3)_{(m+n)}$ supercells. All calculations were performed with the Vienna ab initio simulation program (VASP; Kresse et al. 1993, Kresse and Furthmuller a and b) using ultrasoft Vanderbilt-type plane-wave pseudopotentials (Vanderbilt 1990) with a local density approximation for exchange and correlation energies. Electronic degrees of freedom were optimized with a conjugate gradient algorithm, and both cell constant and ionic positions were fully relaxed. Valence electron configurations for the pseudopotentials are: Ca $6p^26s^2$; Cd $5s^24d^{10}$; Mg $2p^63s^2$; C $2s^22p^2$; O $2s^22p^4$. Total energy calculations were converged with respect to k point meshes; 112 symmetrically distinct k points was typical for 30- or 40-atom triclinic supercells. An energy cutoff of 400 eV was used, in the high precision option which guarantees that *absolute* energies are converged to within a few meV (a few tenths of kJ mol^{-1}; mol = a mole of exchangeable cations; Ca^{2+}, Cd^{2+}, Mg^{2+}).

Results of the FP total energy calculations are listed as formation energies, ΔE_{Str}, in Table 3, which also describes supercell cation configurations. Formation energies are defined such that ΔE_{Str} for a $Ca_mMg_n(CO_3)_{(m+n)}$ supercell with crystal structure *Str* is:

$$\Delta E_{Str}=\frac{E_{Str}-mE_{\alpha}-nE_{\alpha'}}{m+n}\ , \qquad (1)$$

where E_{Str} has units of energy/supercell, but the $\Delta E_{Str}, E_{\alpha}$, and $E_{\alpha'}$ have units of energy/cation. The ΔE_{Str} are compared with calorimetric data (Navrotsky and Capobianco, 1987; Capobianco et al. 1987; Chai et al. 1995) in Figs. 1 and 2. Experimental heats of formation for magnesian calcite with $0 \le X < 0.05$ are lower than a mechanical mixture of calcite plus dolomite (dotted line), which implies a tendency for ordering in this composition range. Explicitly investigating this range with FP calculations requires supercells with at least 100 atoms, and such calculations have not been attempted; one high-symmetry Ca-rich 80-atom supercell calcula-

Table 2 Dolomite-related layer structures

Name	Symbol	X	Space group	[111]-layer sequence	Notation[a]
η	+	$\frac{1}{6}$	$P\bar{3}$	$M^1-C^1-C^2-C^3-C^4-C^5-M^1-\cdots$	$[111]_{C_5M}$
ϵ	□	$\frac{1}{4}$	$R\bar{3}$	$M^1-C^1-C^2-C^3-M^1-\cdots$	$[111]_{C_3M}$
δ	◆	$\frac{1}{3}$	$P\bar{3}$	$C^1-M^1-C^2-C^3-C^4-M^1-C^1-\cdots$	$[111]_{CMC_3M}$
β	■	$\frac{1}{2}$	$R\bar{3}$	$C^1-M^1-C^1-\cdots$ dolomite	$[111]_{CM}$

[a] C = Ca or Cd layer; M = Mg layer

Table 3 Calculated formation energies for $Ca_mMg_n(CO_3)_{(m+n)}$ and $Cd_mMg_n(CO_3)_{(m+n)}$ supercells; all energies are in kJ mol^{-1}

M:N Name Order-type	*T*-matrix[a]			Cation coordinates			Ion Mg = 0	Ca_mMg_n ΔE_{Str} $\Delta E^{b}_{Str'}$	Cd_mMg_n ΔE_{Str} $\Delta E_{Str'}$
2:0	1	0	0	0	0	0	1	0^{Y}	0^{Y}
Calcite	0	1	0	1/2	1/2	1/2	1	0^{Y}	$z0^{Y}$
$\alpha - fcc$	0	0	1						
15:1	2	0	0	0	0	0	0	0.64	
	0	2	0	1/2	0	0	1		
	0	0	2	0	1/2	0	1		
				0	0	1/2	1		
				0	1/2	1/2	1		
				1/2	0	1/2	1		
				1/2	1/2	0	1		
				1/2	1/2	1/2	1		
				1/4	1/4	1/4	1		
				1/4	1/4	3/4	1		
				1/4	3/4	1/4	1		
				3/4	1/4	1/4	1		
				1/4	3/4	3/4	1		
				3/4	1/4	3/4	1		
				3/4	3/4	1/4	1		
				3/4	3/4	3/4	1		
5:1	1	0	0	1/2	3/2	−3/2	1	0.90	1.34
	1	−1	−1	1/2	1/2	−1/2	1		
	−1	2	−1	0	1	−1	1		
				1/2	1/2	−3/2	1		
				1	1	−2	1		
				1	0	−1	0		
5:1	−1	1	0	−1	0	−1	1	0.16	−0.20
η	0	1	−1	−1/2	1/2	−1/2	1		
$[111]_{5:1}$	−1	−1	−1	−3/2	1/2	−3/2	1		
				−3/2	3/2	−3/2	1		
				−1	1	−1	1		
				−2	1	−2	0		
3:1	0	1	−1	−3/2	1/2	1/2	1	1.30^{Y}	1.33^{Y}
	0	−1	0	−1	0	0	1	6.38^{Y}	3.65^{Y}
	−2	1	1	−1/2	1/2	−1/2	1		
				−2	1	0	0		
3:1	1	−1	0	1/2	1/2	1/2	1	-1.65^{Y}	-2.71^{Y}
ϵ	0	1	−1	1	0	0	1	1.92^{Y}	-2.96^{Y}
$[111]_{3:1}$	0	1	1	1/2	1/2	−1/2	1		
				1	1	0	0		
3:1	0	−1	1	1/2	−1/2	3/2	1	4.19^{Y}	-0.12^{Y}
γ	1	0	0	0	0	1	1	6.42^{Y}	-0.50^{Y}
Cu_3Pt	−1	1	1	−1/2	1/2	3/2	1		
				0	0	2	0		
3:1	3/2	−1/2	−1/2	0	0	0	0	44.73	
$\mathcal{H}$	−1/2	3/2	−1/2	0	1	−1	1	−0.09	
Huntite[c]	−1/2	−1/2	3/2	−1	0	1	1		
Cu_3Au				1	−1	0	1		
6:2	1	1	−1	−1	0	−1	1	10.65	6.27
μ	−1	1	1	−1/2	1/2	−1/2	1	10.11	
Cu_3Au	1	−1	1	−3/2	1/2	−3/2	1		
				−3/2	3/2	−3/2	1		
				−1	1	−1	1		
				−1	1	−1	1		
				−1	1	−1	0		
				−2	1	−2	0		
6:2	1	1	−1	−1	0	−1	1	4.60	3.02
ζ	−1	1	1	−1/2	1/2	−1/2	1	9.34	5.90
Al_3Ti	1	−1	1	−3/2	1/2	−3/2	1		
				−3/2	3/2	−3/2	1		
				−1	1	−1	1		
				−1	1	−1	1		

Table 3 Contd.

M:N Name Order-type	*T*-matrix[a]			Cation coordinates			Ion Mg = 0	Ca_mMg_n ΔE_{Str} $\Delta E^{b}_{Str'}$	Cd_mMg_n ΔE_{Str} $\Delta E_{Str'}$
				−1	1	−1	0		
				−2	1	−2	0		
6:2	1	1	−1	−1	0	−1	1	17.03	
ζ^h	−1	1	1	−1/2	1/2	−1/2	1		
Al_3Ti[c]	1	−1	1	−3/2	1/2	−3/2	1		
				−3/2	3/2	−3/2	1		
				−1	1	−1	1		
				−1	1	−1	1		
				−1	1	−1	0		
				−2	1	−2	0		
4:2	−1	1	0	0	2	−1	1	7.50[Y]	6.94[Y]
43	0	0	1	−1/2	3/2	−1/2	1	7.63[Y]	5.14[Y]
48	1	2	−2	0	1	0	1		
				1/2	3/2	−1/2	1		
				1/2	5/2	−3/2	0		
				0	3	−1	0		
4:2	0	1	−1	2	0	−1	1	0.29[Y]	−1.59[Y]
13	0	1	0	3/2	3/2	−3/2	1	5.08[Y]	3.24[Y]
18	3	−1	−1	3	1	−2	1		
				1/2	1/2	−1/2	1		
				5/2	1/2	−3/2	0		
				1	1	−1	0		
4:2	−1	0	1	−1/2	−3/2	1/2	1	8.65[Y]	3.61[Y]
24	−1	1	−1	−1	0	0	1	8.64[Y]	8.14[Y]
28	1	−2	0	−1	−1	0	1		
				−1/2	−1/2	1/2	1		
				0	−1	0	0		
				−1/2	−1/2	−1/2	0		
4:2	1	0	0	1/2	1/2	−1/2	1	0.11[Y]	0.24[Y]
32	1	−1	−1	1/2	1/2	−3/2	1	4.98[Y]	2.12[Y]
37	−1	2	−1	1	1	−2	1		
				1/2	3/2	−3/2	1		
				1	0	−1	0		
				0	1	−1	0		
4:2	1	0	0	0	1	−1	1	7.51[Y]	2.54[Y]
31	1	−1	−1	1/2	1/2	−3/2	1	6.15	6.05
38	−1	2	−1	1	1	−2	1		
				1/2	3/2	−3/2	1		
				1/2	1/2	−1/2	0		
				1	0	−1	0		
4:2	1	0	0	1	0	−1	1	8.00[Y]	2.53[Y]
33	1	−1	−1	1/2	1/2	−3/2	1	7.01[Y]	6.55[Y]
35	−1	2	−1	1	1	−2	1		
				1/2	3/2	−3/2	1		
				1/2	1/2	−1/2	0		
				0	1	−1	0		
4:2	−1	1	0	−1	0	−1	1	−1.23	−1.53
δ	0	1	−1	−3/2	3/2	−3/2	1	−1.64	0.50
$[111]_{CMC_3M}$	−1	−1	−1	−1	1	−1	1		
				−2	1	−2	1		
				−1/2	1/2	−1/2	0		
				−3/2	1/2	−3/2	0		
1:1	1	0	0	0	0	0	1	−3.66[Y]	−4.82[Y]
Dolomite	0	1	0	1/2	1/2	1/2	0		
β – CuPt	0	0	1						
2:2	0	1	−1	−1/2	1/2	−1/2	1	8.27[Y]	2.91[Y]
1	0	−1	0	−1	0	0	1		
	−2	1	1	−3/2	1/2	1/2	0		
				−2	1	0	0		

Table 3 Contd.

M:N Name Order-type	*T*-matrix[a]			Cation coordinates			Ion Mg = 0	Ca_mMg_n ΔE_{Str} $\Delta E^{b}_{Str'}$	Cd_mMg_n ΔE_{Str} $\Delta E_{Str'}$
2:2	1	−1	0	1/2	1/2	1/2	1	−0.38[Y]	−1.50[Y]
4	0	1	−1	1	0	0	1		
	0	1	1	1/2	1/2	−1/2	0		
				1	1	0	0		
2:2	0	−1	1	−1/2	1/2	3/2	1	8.02[Y]	5.60[Y]
v	1	0	0	0	0	1	1		
CuAu	−1	1	1	1/2	−1/2	3/2	0		
				0	0	2	0		
2:2	0	−1	1	−1/2	1/2	3/2	1	8.02[Y]	1.45[Y]
8	1	0	0	0	0	2	1		
	−1	1	1	1/2	−1/2	3/2	0		
				0	0	1	0		
3:3	0	1	−1	1	1	−1	1	10.09[Y]	6.39[Y]
15	0	1	0	3	1	−2	1		
	3	−1	−1	1/2	1/2	−1/2	1		
				2	0	−1	0		
				5/2	1/2	−3/2	0		
				3/2	3/2	−3/2	0		
3:3	−1	0	1	−1/2	−1/2	−1/2	1	5.25[Y]	0.14[Y]
23	−1	1	−1	−1	−1	0	1		
	1	−2	0	−1/2	−1/2	1/2	1		
				0	−1	0	0		
				−1/2	−3/2	1/2	0		
				−1	0	0	0		
3:3	−1	1	0	0	1	0	1	3.13[Y]	2.23[Y]
45	0	0	1	0	3	−1	1		
	1	2	−2	1/2	3/2	−1/2	1		
				0	2	−1	0		
				1/2	5/2	−3/2	0		
				−1/2	3/2	−1/2	0		

[a] Matrix T defines supercell lattice constants, relative to rhombohedral calcite [$R\bar{3}c$ cell constants: *a and* α; Ca: (0, 0, 0); C: (1/4, 1/4, 1/4); O: (x, $1/2 - x$, 1/4), $x = 0.507$] (Megaw 1973). Such that the inverse of the transpose of T, $t \equiv [T^t]^{-1}$, transforms listed cation coordinates (column 3) into fractional supercell coordinates, e.g. for δ phase:

$$T = \begin{vmatrix} -1 & 1 & 0 \\ 0 & 1 & -1 \\ -1 & -1 & -1 \end{vmatrix} \Rightarrow [T^t]^{-1} \bullet \begin{vmatrix} -1 \\ 0 \\ -1 \end{vmatrix}$$

$$= \begin{vmatrix} -2/3 & 1/3 & 1/3 \\ 1/3 & 1/3 & -2/3 \\ -1/3 & -1/3 & -1/3 \end{vmatrix} \bullet \begin{vmatrix} -1 \\ 0 \\ -1 \end{vmatrix} = \begin{vmatrix} 1/3 \\ 1/3 \\ 2/3 \end{vmatrix}$$

[b] ΔE_{Str} is the formation energy for a $Ca_mMg_n(CO_3)_{(m+n)}$ supercell, and $\Delta E_{Str'}$ is for the complimentary $Ca_nMg_m(CO_3)_{(m+n)}$ supercell: $\Delta E_{\epsilon} = -1.65$ kJ mol^{-1} for $Ca_3Mg(CO_3)_4$; $\Delta E_{\epsilon'} = 1.92$ kJ mol^{-1} for $CaMg_3(CO_3)_4$

[c] Huntite, $\mathcal{H}' = CaMg_3(CO_3)_4$, and ζ^h exhibit $CuAu_3$-type ordering of CO_3 groups in addition to $CuAu_3$-type cation ordering in $\mathcal{H}'$, and Al_3Ti-type cation ordering in ζ^h

[Y] The Y (Yes) superscript is attached to each ΔE_{Str} and $\Delta E_{Str'}$ that was used to fit the effective cluster interactions (ECI)

tion was performed, but it has a positive formation energy, $\Delta E_{80} = 0.64$ kJ mol^{-1}.

First-principles phase-diagram calculations

Fitting the cluster expansion

The cluster expansion (CE: Sanchez et al. 1984) is a compact representation of the alloy's configurational total energy. In the quasibinary systems studied here, the alloy configuration is described by pseudospin occupation variables σ_i, which take values −1 or +1 depending upon which cation occupies site i; $\sigma_i = -1$ for Ca or Cd, $\sigma_i = +1$ for Mg.

The CE parametrizes the configurational energy (per exchangeable atom; Ca, Mg, Cd) as a polynomial in pseudospin occupation variables:

$$E(\sigma) = \sum_{\ell} m_{\ell} J_{\ell} \left\langle \prod_{i \in \ell'} \sigma_i \right\rangle \ , \qquad (2)$$

where ℓ is the cluster defined by the set of sites $\{i\}$. The sum is taken over all clusters ℓ that are not symmetrically equivalent in the parent structure space group, and the average is taken over all clusters ℓ' that are sym-

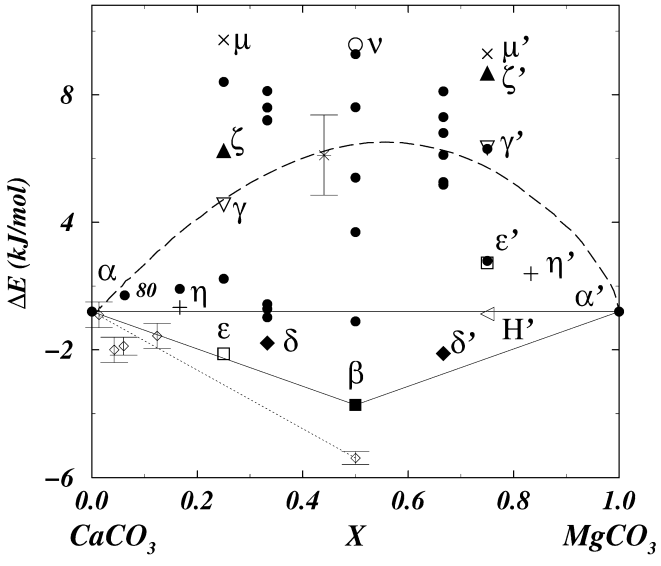

Fig. 1 $CaCO_3$–$MgCO_3$. Comparison of VASP-calculated formation energies ΔE_{Str}, (*Str* indexes a crystal structure and X = mol fraction $MgCO_3$) with experimental heats of formation. ◇ *with error bars* Navrotsky and Capobianco (1987) data; *dotted line* connects calcite with the lowest-energy measurement for dolomite; * *with error bars* is data of Chai et al. (1995) for their most disordered dolomite sample; the *dashed line* is the FPPD calculated total energy for a random solid solution, $\Delta E_{Rand}(X)$; the *solid line* connects predicted ground-state structures: α calcite; β dolomite; α' magnesite

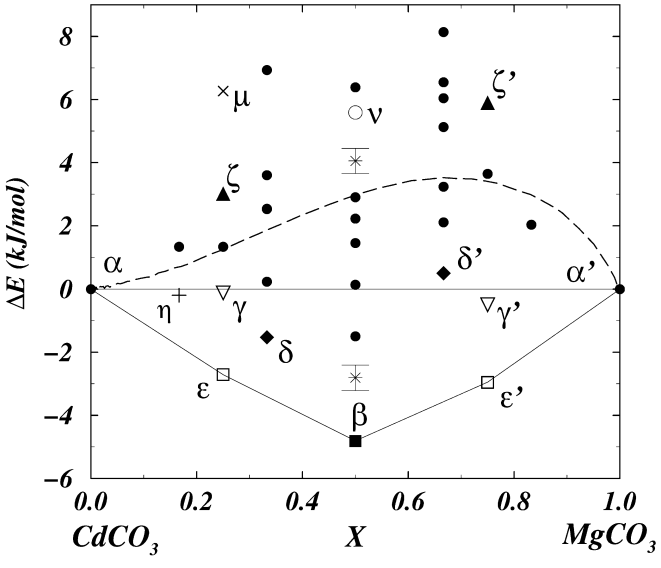

Fig. 2 $CdCO_3$–$MgCO_3$. Comparison of VASP-calculated formation energies ΔE_{Str}, experimental heats of formation. * *with error bars* Data of Capobianco et al. (1987) for maximally ordered, and disordered β-phase; the *dashed line* is the FPPD-calculated total energy for a random solid solution, $\Delta E_{Rand}(X)$; the *solid line* indicates predicted ground-state structures: α calcite; ϵ $[111]_{C_3M}$; β dolomite; ϵ' $[111]_{CM_3}$; α' magnesite

metrically equivalent to ℓ. Coefficients J_ℓ are called effective cluster interactions (ECI), and the multiplicity of a cluster, m_ℓ, is the number of symmetrically equivalent clusters, divided by the number of cation sites. The ECI are obtained by fitting a set of FP-calculated structure energies, $\{E_{Str}\}$. The resulting CE can be improved as necessary by increasing the number of clusters ℓ and/or the number of E_{Str} used in the fit.

Fitting was performed with the MIT ab-initio phase stability software package (MAPS; Van de Walle 1999) which automates most of the tasks associated with the construction of a CE Hamiltonian. A complete description of the algorithms underlying the code can be found in Van de Walle and Ceder (2002). The most important steps are: (1) selecting which FP structure energies to calculate, which MAPS does in a way that minimizes the statistical variance of the estimated ECI; (2) automatically selecting which clusters to include in the expansion by minimizing the cross-validation score, CV:

$$(\mathrm{CV})^2 = \frac{1}{N}\sum_{Str=1}^{N}(E_{Str} - \hat{E}_{-Str})^2 \qquad (3)$$

where $E_1, \ldots E_N$ denote the structure energies calculated from FP and E_{-Str} is the energy of structure *Str* predicted from a CE fitted to the remaining $N-1$ energies. This criterion ensures that the chosen set of clusters maximizes the predictive power of the CE for any structure, whether or not it is included in the fit. (In contrast, the standard mean-squares error criterion minimizes the error only for structures included in the fit.) In addition to the CV criterion, the code also ensures that ground states predicted from the CE agree with the minimum energy structures for each composition, as calculated from FP. The code proceeds by iterative refinement, gradually increasing the number of clusters and the number of structures to provide the best possible fit based on the set $\{E_{Str}\}$ calculated so far.

For this study, MAPS was run until CE precision reached CV = 0.015 meV cation^{-1} for the $CaCO_3$–$MgCO_3$ system and CV = 0.019 meV cation^{-1} for $CdCO_3$–$MgCO_3$. Achieving this accuracy required calculation of the 27 E_{Str} that are marked by the superscript Y (as in Yes) in Table 3.

The end result of this procedure is a set of ECI, $\{J_{(r,t)}\}$, which define the interactions associated with r-body clusters of types t. Fitted ECI sets for $CaCO_3$–$MgCO_3$ and $CdCO_3$–$MgCO_3$ are listed in Table 4, and the products of effective pair interactions [EPI; $J_{(2,t)}$] and their multiplicities, $m_{(r,t)}$, are plotted in Fig. 3. • = values for $CaCO_3$–$MgCO_3$; □ = values for $CdCO_3$–$MgCO_3$. As postulated by Burton and Kikuchi (1984), $J_{(2,1)}$, the nearest-neighbor (*nn*) interlayer pair interaction favors ordering, while $J_{(2,2)}$, the *nn* intralayer interaction favors phase separation; note that the sign convention is reversed relative to Burton and Kikuchi (1984); here, $J_{(2,1)} > 0$ favors ordering and $J_{(2,2)} < 0$ favors phase separation.

Ground-state analysis

Ground-state (GS) analyses were performed by brute force enumeration of all ordered configurations with 60

Table 4 Effective cluster interactions in kJ mol^{-1}

Rhombohedral cluster coordinates minus (0,0,0)	$m(r, t)$ Multiplicity	$CaCO_3$–$MgCO_3$	$CdCO_3$–$MgCO_3$
Zero cluster	1	13.150425	5.957591
Point cluster	2[a]	1.862754	2.741019
(1/2,−1/2,1/2)	6	0.450299	1.208615
(0,−1,1)	6	−1.828504	−1.649628
(1/2,−3/2,1/2)	6	0.313948	0.674401
(1,0,0)	6	−0.283364	0.056055
(−3/2,3/2,−1/2)	12	−0.619792	−0.574350
(1,1,−1)	6	0.016498	
(1,−2,1)	6	−0.452398	
(−1/2,0,−1/2), (−1/2,−1/2,1/2)	12	−0.390458	−0.26610
(−1,0,1), (0,−1,1)	4	0.624520	−0.38727

[a] 2 is the multiplicity of cations in the $Z = 2$ rhombohedral cell

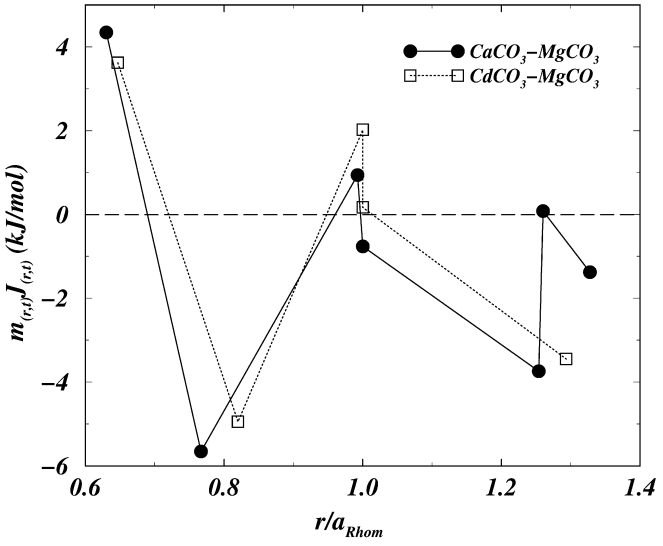

Fig. 3 Effective pair interactions, $J_{(2,t)}$, multiplied by their multiplicities, $m_{(r,t)}$, for • $CaCO_3$–$MgCO_3$ and □ $CdCO_3$–$MgCO_3$. The sign convention is: $J_{(2,1)} > 0$ implies that interlayer ordering is energetically favorable; $J_{(2,2)} < 0$ implies that intralayer ordering is energetically unfavorable (as postulated by Burton and Kikuchi 1984)

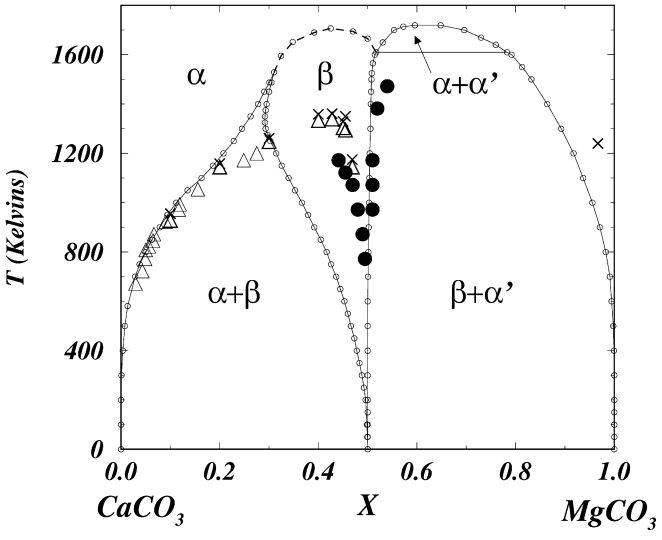

Fig. 4 Calculated $CaCO_3$–$MgCO_3$ phase diagram (*solid* and *dashed lines through small open circles*). Experimental phase boundary data are from Goldsmith (1983) and references therein

or fewer atoms per supercell (12 or fewer cation sites). These analyses did not predict any new GS configurations besides those shown in Figs. 1 and 2. In addition, Monte Carlo (MC) simulations described below revealed no other GS, strongly suggesting that our GS search is exhaustive.

Monte Carlo phase diagram calculations

The MAPS package includes a companion MC code (described in A. Van de Walle and M. Asta) that was used to calculate the $CaCO_3$–$MgCO_3$ and $CdCO_3$–$MgCO_3$ phase diagrams (Figs. 4,5). This code implements semigrand canonical MC simulations, in which the total number of atoms is fixed and the chemical concentration varies in response to a fixed difference in the chemical potentials of the two cation species. Phase boundaries at a given temperature were found by scanning a range of imposed chemical potential values while monitoring the concentration in the simulation cell. Phase transitions were located by identifying discontinuities in the concentration. Values of the concentration just before and just after the discontinuity bracketed the equilibrium concentrations of coexisting phases at the transition.

Convergence with respect to system size was tested by calculating T_c for the $\beta \rightleftharpoons \alpha$, dolomite⇌calcite, order–disorder transition, and a system of $12 \times 12 \times 12$ supercells (3465 cation sites) was selected for all MC calculations. Thermodynamic functions of interest, such as concentration, were obtained by averaging over 1500 MC passes for each value of chemical potential and temperature. Temperature and chemical potential were scanned in increments of 5 K and 0.01 eV $atom^{-1}$, respectively. After each detected phase transition, the system was reequilibrated for 1500 MC passes before the

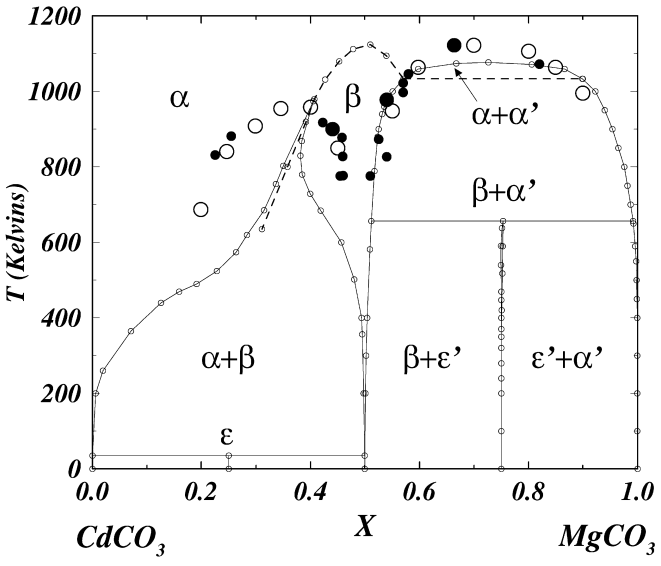

Fig. 5 Calculated $CdCO_3$–$MgCO_3$ phase diagram (*solid* and *dashed lines through small open circles*); *large open circles* and *filled circles* data from Goldsmith and Heard (1972)

process of locating the phase boundary at the next temperature was initiated.

Discussion

Equilibrium phase relations: comparison with experiment

Qualitatively, there are no discrepancies between calculated and experimental phase diagrams. The unobserved ϵ, and ϵ' phases in $CdCO_3$–$MgCO_3$ are predicted to occur only at temperatures below the lowest that were investigated experimentally. Predicted values for the critical temperatures of $\beta \rightleftharpoons \alpha$ order–disorder transitions at $X = 0.5$ are: $T_C(Predicted)/T_C \approx 1.16 \pm 0.03$ for $CaCO_3$–$MgCO_3$, and $T_C(Predicted)/T_C \approx 1.04 \pm 0.02$ for $CdCO_3$ –$MgCO_3$. Typically, FPPD calculations overestimate transition temperatures especially when, as here, vibrational effects are ignored; e.g. $T_C(Predicted)/T_C \approx 1.32$ for the compound CdMg (Asta et al. 1993).

Solubilities of Ca or Cd in the dolomite structure β phases are significantly overestimated. In addition, the predicted $CaCO_3$–$MgCO_3$ homogeneity range for α' is enhanced, and the field for two Mg-rich disordered phases is reduced, relative to the experimental diagram.

Metastable phase relations: magnesian calcite and calcian dolomite

Assuming that cation ordering is the only relevant process, the ΔE_{Str} results plus the $\Delta E_{Rand}(X)$ curve (dashed line, Fig. 4, provide a substantially improved basis for interpreting metastable phase relations in magnesian calcite and calcian dolomite (Wenk et al. 1991). Metastable ordered phases have a driving force for formation only if their free energies are lower than that of the disordered solution from which they might form; i.e. $F_{Ord} < F_{Rand}$ is a necessary, but not sufficient, condition for metastable formation. Because the random state has greater configurational entropy than any ordered configuration (or a disordered phase with short-range order), it will therefore have lower free energy than any ordered state of equal or higher formation energy, at finite temperature. It follows that:

$$\Delta E_{Ord} > \Delta E_{Rand} \Rightarrow F_{Ord} > F_{Rand} \quad , \tag{4}$$

which implies that $\Delta E_{Ord} < \Delta E_{Rand}$ is a necessary condition for an ordered phase to be a candidate for metastable formation. Thus, all phases with $\Delta E_{Str} > \Delta E_{Rand}(X)$ (μ, ν, ζ), or $\Delta E_{Str} \approx \Delta E_{Rand}(X)$, (γ) are poor candidates for metastable formation. These results clearly contradict all proposed models of ordering in magnesian calcite with $X \approx \frac{1}{4}$: (1) the proposal of Wenk et al. (1991) that **c** reflections in magnesian calcite might be caused by ν-type ordering; (2) predictions of Burton (1987) and Burton and Davidson (1988) that a μ- or ζ-type ordering, or a combination of the two, might actually be associated with a stable or metastable low-temperature phase. Except for huntite (see below) the lowest-energy metastable states are all dolomite-related layer structures: δ, $[111]_{CMC_3M}$; ϵ, $[111]_{C_3M}$; η, $[111]_{C_5M}$ (Table 1). From an energetic perspective, it is surprising that ϵ-type ordering has not been reported in magnesian calcite; ϵ is predicted to be very nearly stable, and it is substantially more stable than any of the previously predicted candidates.

Predictions of Burton (1987) "that $Ca_3Mg(CO_3)_4$ is probably stable at low temperature," meaning that a phase with μ- or ζ-type cation order, or a combination of the two (Burton and Davidson 1988), are apparently wrong. This prediction was based on a cluster variation method (CVM: Kikuchi 1951) calculation in the tetrahedron approximation (TA), that could only include the first two EPI [$J_{(2,1)}$ and $J_{(2,2)}$], *nn* interlayer and intralayer pair interactions, plus one three-body term. The Hamiltonian fit by MAPS, however, includes the first seven EPI plus two three-body terms. Clearly, the CVM TA is not sufficient for this system because the largest clusters it includes are too small, and this demonstrates the advantage of using MC simulation for FPPD calculations; MC calculations easily handle relatively long-range interactions, whereas CVM expansions typically become intractable when interaction range exceeds third or fourth *nn*.

Wenk et al. (1991) used a concentration wave (CW) analysis (Khachaturyan 1978; Khachaturyan and Pokrowskii 1985; Khachaturyan et al. 1988) as a basis for discussing metastable phase relations between α, β, γ, δ, μ, and ν, phases (ignoring ϵ and ζ). The CW criterion for a plausible transition between two phases (e.g. $\beta \rightarrow \gamma$) is that the two crystal structures are sufficiently similar to be related by a "simple instability;" i.e. by an infinites-

imal perturbation in the amplitude of one ordering CW which reduces the free energy of the system. This criterion combines two concepts: (1) structural similarity; (2) instability with respect to a change in ordering. Instability implies a negative second derivative of the free energy with respect to at least one order parameter, i.e. one CW. The CW analysis, however, provides no Hamiltonian with which to evaluate formation energies, free energies, or instabilities, and these are severe limitations. Also, the $\alpha \rightarrow \epsilon$ reaction is associated with a "simple instability," $\mathbf{k}_\epsilon = \frac{2\pi}{a}[\frac{1}{3}(111)_{fcc}]$ in the notation of Wenk et al. (1991), and because its energy is so low, one would expect it to form readily. However, ϵ is associated only with unobserved **d** reflections ($hkl : -h + k + l \neq 3n$, Table 2 in Van Tendeloo et al. 1985) rather than the observed **c** reflections.

The FPPD results establish an energy hierarchy which rules out most proposed metastable ordering processes: e.g. $\Delta E_\gamma \approx \Delta E_{Rand}$, and $\Delta E_\beta \gg \Delta E_\delta$, so $\beta \rightarrow \gamma$ in calcian dolomite is a highly unlikely reaction, but $\beta \rightarrow \delta$ is highly plausible. Some caveats related to CO_3-group disorder and impure samples: (1) CO_3-group disorder would increase the energy of disordered magnesian calcite, or metastable calcian dolomite, and this could make some high-energy states accessible as metastable reaction products. CO_3-group disorder in magnesian calcite is plausible because the 1260-K order–disorder transition temperature (Dove and Powell 1989) implies energetics that are comparable to cation order–disorder; however, disordered natural samples with higher energy than ΔE_{Rand} have not been reported. (2) Natural samples that exhibit sharp **c** reflections with streaking (Wenk et al. 1991) are very Fe-rich, $Ca_{0.5}Mg_{0.2}Fe_{0.3}CO_3$, which may have a significant effect on their energetics. Samples of composition $Ca_{0.95}Mg_{0.05}CO_3$ also exhibit **c** reflections, but they are more diffuse, and streaking is not observed.

Huntite, $CaMg_3(CO_3)_4$

Huntite ($\mathcal{H}'$, in Fig. 1) is observed in nature (Graf and Bradley 1962), and it exhibits Cu_3Au-type ordering of both cation and CO_3 anion-group orientations. Huntite's $CaMg_3(CO_3)_4$ stoichiometry is in a region of the phase diagram in which dolomite- plus magnesite-based solid solutions coexist, so it is clearly metastable. This is consistent with the FP results; $\Delta E_{\mathcal{H}'}$ is lower than any other ΔE_{Str} at $CaMg_3(CO_3)_4$ stoichiometry (Fig. 1). Note, however, that the CE-based GS analysis does not include huntite, or any other structure(s) with orientationally ordered anion groups. Therefore, the prediction that huntite is the lowest-energy metastable state at $CaMg_3(CO_3)_4$ stoichiometry is weaker than it would be if CO_3 group orientational order was included in the Hamiltonian and GS search. For completeness, the formation energy of huntite structure $Ca_3Mg(CO_3)_4$ was also calculated; $\Delta E_{\mathcal{H}} = 44.73$ kJ mol^{-1} (Table 3).

Predicted phases in $CdCO_3$–$MgCO_3$

In the $CdCO_3$–$MgCO_3$ system, both the ϵ and ϵ' phases are predicted to be stable, but neither has been observed experimentally. This does not contradict experiment however, because the highest temperature at which ϵ' is predicted to be stable is ~650 K, which is ~40 K below the lowest temperature experiments reported in Goldsmith and Heard (1972).

Conclusions

The results presented above demonstrate semiquantitative agreement between FPPD calculations and experimental phase equilibria and thermochemical data. They also provide an energetic hierarchy that can be used to evaluate the plausibilities of proposed metastable reaction paths. Specifically, the FP and FPPD results presented above appear to rule out the proposed metastable formation of γ or ν in magnesian calcite, unless the magnesian calcite is disordered with respect to both cation ordering and CO_3-group orientation. Low-temperature ϵ and ϵ' phases are predicted in the $CdCO_3$–$MgCO_3$ system.

Acknowledgements This work was partially supported by NSF contract DMR-0080766 and NIST.

References

Asta M, McCormack R, de Fontaine D (1993) Theoretical study of alloy phase stability in the Cd–Mg system. Phys Rev (B) 48: 748–766

Burton BP (1987) Theoretical analysis of cation ordering in binary rhombohedral carbonate systems (at the end of this paper there is a "note added in proof"). Am Mineral 72: 329–336

Burton BP, Kikuchi R (1984) Thermodynamic analysis of the system $CaCO_3$–$MgCO_3$ in the tetrahedron approximation of the cluster variation method. Am Mineral 69: 165–175

Burton BP, Davidson PM (1988) Multicritical phase relations in minerals. In: Ghose S, Coey JMD, Salje E (eds) Advances in physical geochemistry, vol. 7. Springer, Berlin Heidelberg New York, pp 60–90

Capobianco C, Burton BP, Davidson PM, Navrotsky A (1987) Structural and calorimetric studies of order–disorder in $CdMg(CO_3)_2$. J Solid State Chem 79: 214–223

Chai L, Navrotsky A, Reeder RJ (1995) Energetics of calcium-rich dolomite. Geochem Cosmochem Acta 59[5]: 939–944

Davidson PM (1994) Ternary iron, magnesium, calcium carbonates: a thermodynamic model for dolomite as an ordered derivative of calcite-structure solutions. Am Mineral 79: 332–339

Dove MT, Powell BM (1989) Neutron diffraction study of the tricritical orientational order/disorder phase transition in calcite at 1260 K. Phys Chem Miner 16: 503–507

Goldsmith JR (1983) Phase relations of rhombohedral carbonates. In: Reeder RJ (ed) Reviews in mineralogy, vol. 11. Mineralogical Society of America, Washington DC, pp 49–76

Goldsmith JR, Heard HC (1961) Subsolidus phase relations in the system $CaCO_3$–$MgCO_3$. J Geol 69: 45–74

Goldsmith JR (1972) Cadmium dolomite and the system $CdCO_3$–$MgCO_3$. J Geol 80: 611–626

Graf DL, Bradley WF (1962) The crystal structure of huntite, $Mg_3Ca(CO_3)_4$. Acta Crystallogr 15: 238–242

Khachaturyan AG (1978) Ordering in substitutional and interstitial solid solutions. Prog Mater Sci 22: 1–150
Khachaturyan AG, Pokrowskii BI (1985) Concentration wave approach in structural and thermodynamic characterization of ceramic crystals. Prog Mater Sci 29: 1–138
Khachaturyan AG, Lindsley TF, Morris JW (1988) Theoretical investigation of precipitation of δ' in Al–Li. Metall Trans 19A: 249–258
Kikuchi RA (1951) A theory of cooperative phenomena. Phys Rev 81: 988–1003
Kresse G, Hafner J (1993) Ab initio molecular dynamics for liquid metals. Phys Rev (B) 47: 558–561
Kresse G (1994) Doctoral Thesis, Technische Universität Wien 1993. Phys Rev (B) 49: 14 251
Kresse G, Furthmüller J (1996a) Efficiency of ab-initio total energy calculations for metals and semiconductors using a plane-wave basis set. Comput Mat Sci 6: 15–50
Kresse G, Furthmüller J (1996b) Efficient iterative schemes for ab initio total-energy calculations using a plane-wave basis set. Phys Rev (B) 54: 11169 cf. http://tph.tuwien.ac.at/vasp/guide/vasp.html
McCormack RP, Burton BP (1997) Modeling phase stability in $A(B_{1/3}B'_{2/3})O_3$ perovskites, Comp Mater Sci 8: 153–160
Megaw HD (1973) Crystal structures: a working approach. Studies in physics and chemistry, 10. W.B. Saunders Company, Philadelphia, 242 pp
Meike A, Wenk H-R, O'Keefe MA, Gronsky R (1988) Atomic resolution microscopy of carbonates. Interpretation of contrast. Phys Chem Miner 15: 427–437
Navrotsky A, Capobianco C (1987) Enthalpies of formation of dolomite and magnesian calcite. Am Mineral 79: 782–787
Navrotsky A, Louks D (1977) Calculation of subsolidus phase relations in carbonates and pyroxenes. Phys Chem Miner 1: 109–127
Reksten K (1990a) Modulated microstructures in calcian ankerites. Am Mineral 75: 495–500
Reksten K (1990b) Superstructures in calcite. Am Mineral 75: 807–812
Reksten K (1990c) Superstructures in calcian ankerites. Phys Chem Miner 17: 266–270
Sanchez JM, Ducastelle F, Gratias D (1984) Generalized cluster description of multicomponent systems. Physica 128(A): 334–350
Van de Walle A (1999) MAPS: the MIT ab initio phase stability code http://www.mit.edu/~avdw/maps/
Van de Walle A, Ceder G (2002) Automating first-principles phase diagram calculations, Journal of Phase Equilibria, 23 p. 348
Van de Walle A, Asta M (2002) Self-driven lattice-model Monte Carlo simulations of alloy thermodynamic, Modelling and Simulations in Materials Science and Engineering 10 p. 521
Vanderbilt D (1990) Soft self-consistent pseudopotentials in a generalized eigenvalue formalism Phys Rev (B) 41: 7892–7895
Van Tendeloo G, Wenk HR, Gronsky R (1985) Modulated structures in calcian dolomite: a study of electron microscopy. Phys Chem Miner 12: 333–341
Wenk H-R, Zhang F (1985) Coherent transformations in calcian dolomites. Geology 13: 457–460
Wenk H-R, Meisheng Hu, Lindsley T, Morris JW Jr. (1991) Superstructures in ankerite and calcite. Phys Chem Miner 17: 527–539